Organic Electronics xxx (xxxx) xxx

Contents lists available at ScienceDirect

Organic Electronics

journal homepage: http://www.elsevier.com/locate/orgel

Linear-shaped thermally activated delayed fluorescence emitter using 1,5-naphthyridine as an electron acceptor for efficient light extraction

Youngnam Lee [a], Seung-Je Woo [b], Jang-Joo Kim [b,**], Jong-In Hong [a,*]

[a] Department of Chemistry, Seoul National University, Seoul, 08826, Republic of Korea
[b] Department of Materials Science and Engineering, Seoul National University, Seoul, 08826, Republic of Korea

ARTICLE INFO

Keywords:
Organic light emitting diode
Thermally activated delayed fluorescence
Light out coupling efficiency
Emitting dipole orientation
Naphthyridine

ABSTRACT

In this study, we developed a donor-π-acceptor-π-donor-type thermally activated delayed fluorescence (TADF) emitter (**NyDPAc**) using 1,5-naphthyridine as a core moiety. **NyDPAc** exhibited a high horizontal dipole ratio and thus a high external quantum efficiency (20.9%) even at a relatively low photoluminescence quantum yield (57%). 1,5-naphthyridine as an electron acceptor represents a promising core moiety for efficient TADF materials.

1. Introduction

Organic light-emitting diodes (OLEDs) have attracted considerable attention as a future display technology. Phosphorescence emitters can attain 100% of the internal quantum efficiency (IQE) due to the strong spin-orbit coupling of heavy metals [1,2], as compared to conventional fluorescence emitters that yield only 25% of the IQE [3,4]. However, because iridium and platinum used in phosphorescence emitters are rare-earth elements and expensive, considerable effort has been devoted to developing pure organic emitters which can reach 100% of the IQE.

Recently, thermally activated delayed fluorescence (TADF) materials have received a great deal of attention as alternative OLED emitters [5–10]. TADF emitters require a small singlet-triplet energy gap (ΔE_{ST}) and have shown a maximum photoluminescence quantum yield (PLQY) of 100% when triplet (T_1) excitons are fully converted to singlet (S_1) excitons through reverse intersystem crossing (RISC). For high efficiency OLEDs, both the IQE and external quantum efficiency (EQE) should be considered, where the EQE is related to light out-coupling [11]. Even when the IQE of TADF materials reaches 100%, the theoretical maximum EQE is only 20% for isotropic materials due to limited light out-coupling efficiencies [12,13]. Therefore, designing emitters which can fully extract electroluminescence through the glass substrate is necessary. These materials tend to be highly linear or planar, the dipoles of which are aligned horizontally when thermally deposited [14].

In general, TADF materials can be designed by reducing the ΔE_{ST} through distortion of electron donors and acceptors. Despite many efficient TADF materials based on combinations of electron donors and acceptors, OLED device efficiencies containing these emitters with near-unity PLQYs are insufficient due to low light out-coupling efficiencies [15–17]. Efficiency of TADF materials can be enhanced by employing linear-shaped fluorescent molecules with a horizontal orientation. There have been some reports about TADF emitters exhibiting a high horizontal dipole ratio using triscarbazole, tri-spiral electron donor, spiro-linked double electron donors and acceptors, and others [18–22]. However, to the best of our knowledge, 1,5-naphthyridine has not been used as a core moiety for linear-shaped TADF molecules showing excellent high horizontal dipole ratios.

1,5-naphthyridine has been known for its applications in pharmaceutical communities [23–25]. However, applications to OLEDs as an electron acceptor remain largely unexplored. In this study, we designed a linear-shaped TADF emitter (**NyDPAc**) by connecting 1,5-naphthylidine as an electron acceptor and dimethylacridine as an electron donor through a phenylene bridge (Fig. 1a). **NyDPAc** showed TADF emission due to the orbital separation between the electron donor and acceptor. Furthermore, the rod-like structure of **NyDPAc** induced horizontal deposition during thermal evaporation, resulting in maximized light out-coupling efficiency. Thus, the **NyDPAc**-based OLED device showed a high EQE of 20.9% despite a relatively low PLQY (57%). This is the first case of utilizing 1,5-naphthyridine as a linear acceptor for achieving high TADF OLED efficiency.

* Corresponding author.
** Corresponding author.
E-mail addresses: jjkim@snu.ac.kr (J.-J. Kim), jihong@snu.ac.kr (J.-I. Hong).

https://doi.org/10.1016/j.orgel.2019.105600
Received 10 September 2019; Received in revised form 23 November 2019; Accepted 17 December 2019
Available online 18 December 2019
1566-1199/

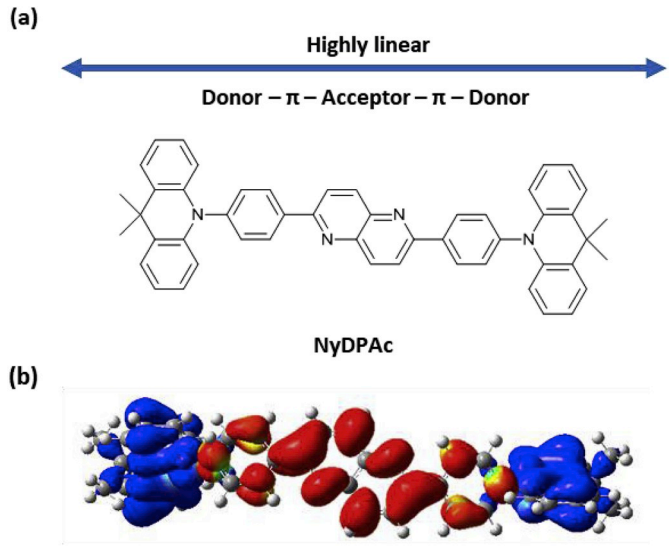

Fig. 1. (a) Design strategy (b) optimized geometry: HOMO (blue), LUMO (Red). (For interpretation of the references to color in this figure legend, the reader is referred to the Web version of this article.)

2. Experimental

2.1. Quantum chemical calculations

All quantum chemical calculations were performed using the Gaussian '09 program package. Gas-phase geometry optimizations for the lowest excited singlet and triplet states were carried out using density functional theory (DFT) and time-dependent density functional theory (TD-DFT) calculations at the B3LYP/6-31G(d) level.

2.2. Photophysical property analysis

UV–visible spectra were recorded on a Jasco V-730 spectrophotometer. Fluorescence and phosphorescence spectra were recorded on a Jasco FP-8300 spectrophotometer. Absolute quantum efficiency was obtained with a PTI QuantaMaster 40 spectrofluorometer using a 3.2 in. integrating sphere at room temperature. Transient photoluminescence (PL) was measured with a streak camera (Hamamatsu Photonics, Japan) using a nitrogen laser (337 nm; Usho Optical Systems, Japan) as the excitation source. For angle-dependent PL (ADPL) measurements, p-polarized light emitted from PL samples was measured by attaching the film substrate to a half-cylinder lens with index-matching oil and changing the angle between the sample and the detector from −90° to 90° using a motorized rotational stage.

2.3. Electrochemical and thermal analysis

Cyclic voltammetry (CV) experiments were conducted in DMF solution (1.00 mM) with 0.1 M tetra-*n*-butylammonium perchlorate (TBAP) as the supporting electrolyte. A glassy carbon electrode was employed as the working electrode and referenced to an Ag reference electrode. All potential values were calibrated against the ferrocene/ferrocenium (Fc/Fc^+) redox couple. The onset potential was determined from the intersection of two tangents drawn at the rising and background current of the cyclic voltammogram. Differential scanning calorimetry (DSC) and thermogravimetric analysis (TGA) were performed with a TA instrument DSC Q10 and Q50 thermogravimetric analyzer in a nitrogen atmosphere at a heating rate of 10 °C min^{-1}.

Table 1
Calculated data of **NyDPAc**.

	HOMO [eV]	LUMO [eV]	E_{gap} [eV]	S_1 [eV]	T_1 [eV]	ΔE_{ST} [eV]
NyDPAc	4.90 eV	2.22 eV	2.68 eV	2.286 eV	2.282 eV	0.004 eV

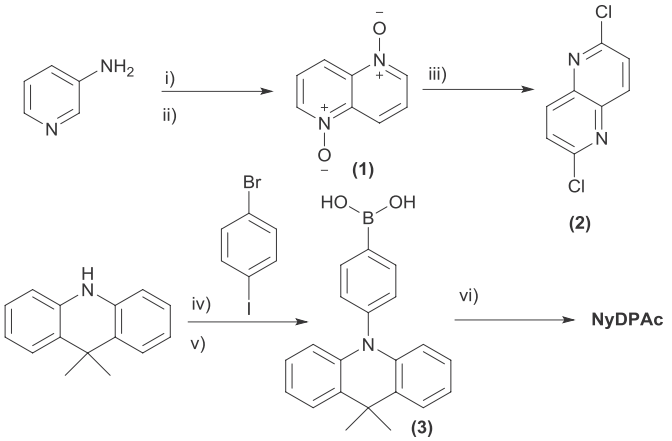

Scheme 1. Synthetic routes for NyDPAc. i) *m*-NO_2PhSO_3Na, glycerol, H_2SO_4, H_2O, 150 °C; ii) mCPBA, CH_2Cl_2/MeOH, rt; iii) $POCl_3$, 110 °C, 20 min; iv) CuI, *trans*-1,2-cyclohexanediamine, sodium *tert*-butoxide, 1,4-dioxane, 100 °C; v) *n*-BuLi, trimethyl borate, THF, −78 °C → rt; vi) $Pd(PPh_3)_4$, K_2CO_3, 1,4-dioxane/H_2O, 100 °C.

2.4. Device fabrication and measurements

The patterned indium-tin-oxide (ITO, 150 nm) substrates were washed with water and isopropyl alcohol, followed by 10 min UV-ozone treatment. Organic layers, LiF, and Al were thermally evaporated at a deposition rate of 1–2 Å s^{-1} for organic layers, 0.1 Å s^{-1} for LiF, and 3–5 Å s^{-1} for the Al electrode. OLED properties were measured using a Keithley source meter 2400 and a PR-650 spectrascan colorimeter.

2.5. Synthesis and characterization

Commercially available reagents and solvents were used without further purification unless otherwise noted. ^1H and ^{13}C NMR spectra were recorded using an Agilent 400-MR DD2 400 MHz or Varian/Oxford As-500 500 MHz in $CDCl_3$. ^1H NMR chemical shifts in $CDCl_3$ were referenced to $CHCl_3$ (7.27 ppm). ^{13}C NMR chemical shifts in $CDCl_3$ were reported relative to $CHCl_3$ (77.23 ppm). Mass spectra were recorded on a matrix-assisted laser desorption ionization time-of-flight (MALDI-TOF) Microflex instrument from Bruker. High-resolution mass spectrometric (HRMS) data (JEOL, JMS-700) with fast atom bombardment (FAB) positive mode were received directly from the National Center for Inter-University Research Facilities (NCIRF). Elemental analyses were carried out using Thermo Scientific FlashEA 1112.

3. Results and discussion

3.1. Theoretical calculations

DFT and TD-DFT calculations of **NyDPAc** were performed to show an optimized molecular structure and the highest occupied molecular orbital (HOMO)/lowest unoccupied molecular orbital (LUMO) of ground states and energies of excited states at the B3LYP/6-31G(d) level. The calculated data are summarized in Table 1. DFT calculations of **NyDPAc** revealed a linear shape as the optimized geometry (Fig. 1b), where dimethylacridine and a phenylene bridge were distorted with a

Table 2
Physical and photophysical data of **NyDPAc**.

	λ_{PL}[a/b] [nm]	E_S[a/b] [eV]	E_T[a/b] [eV]	ΔE_{ST}[a/b] [eV]	PLQY[b] [%]	τ_F[b] [ns]	τ_{TADF}[b] [μs]	HOMO[c] [eV]	HOMO[c] [eV]	$\theta_{//}$[d] [%]	T_g[e]/T_d[f] [°C]
NyDPAc	486/510	2.81/2.80	2.51/2.51	0.30/0.29	57	12	451	5.30	2.87	92	144/414

[a] Measured using toluene solution (10^{-5} M).
[b] Measured using 10 wt% **NyDPAc** doped in DPEPO film.
[c] Estimated from the onset potentials ($^{ox}E_{onset}$ and $^{red}E_{onset}$ [eV] against F_c/F_{c+} redox couple) in CV experiments.
[d] The horizontal emitting dipole ratio.
[e] The glass transition temperature.
[f] The temperature at 5% weight loss.

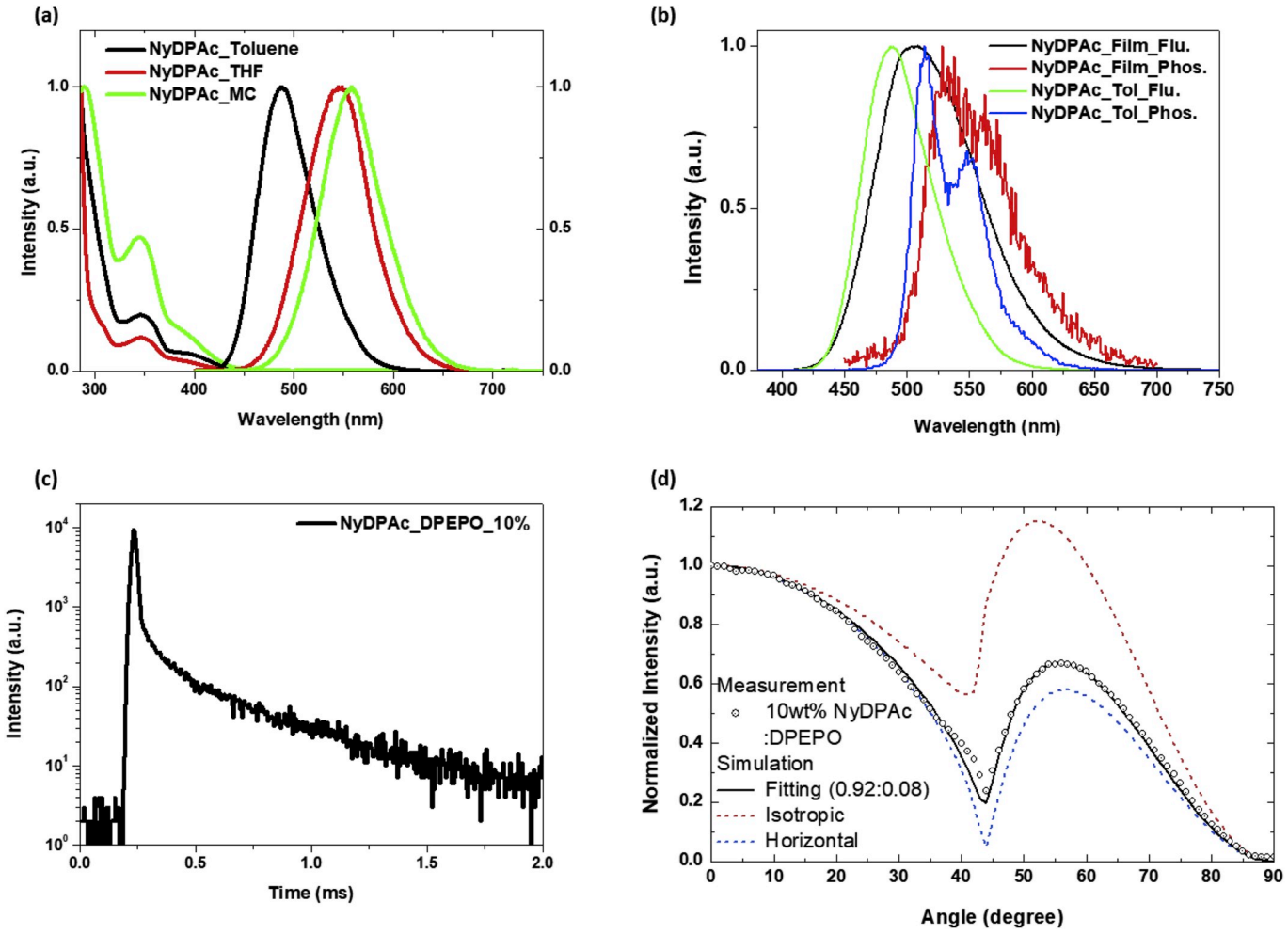

Fig. 2. (a) Absorption and PL spectra of **NyDPAc** in solution (concentration: 10^{-5} M). (b) Fluorescence and phosphorescence spectra of **NyDPAc** in toluene and 10 wt % **NyDPAc** doped in DPEPO film. (c) Transient PL decay curve using 10-wt% **NyDPAc** doped in DPEPO film. (d) Angle-dependent PL intensity.

dihedral angle of 89° because of steric hindrance. The HOMO was localized on the dimethylacridine moiety, whereas the LUMO was localized on the linear core of 1,5-naphthyridine and two phenylene linkers. The energies of singlet (2.286 eV) and triplet (2.282 eV) excited states were estimated using TD-DFT calculations, resulting in a small ΔE_{ST} of 0.004 eV.

3.2. Synthesis

The synthetic procedure is depicted in Scheme 1. First, 3-aminopyridine was heated with sulfuric acid, glycerol, and 3-nitrobenzene sulfonate to produce 1,5-naphthyridine through a Skraup reaction. The resulting 1,5-naphthyridine was oxidized with mCPBA to yield 1,5-naphthyridine-1,5-dioxide (**1**), which was then chlorinated using $POCl_3$ to furnish 2,6-dichloro-1,5-naphthyridine (**2**). 2,6-Bis(4-(9,9-dimethylacridin-yl)phenyl)-1,5-naphthyridine (**NyDPAc**) was obtained through Suzuki-Miyaura coupling between **2** and (4-(9,9-dimethylacridin-10(9*H*)-yl)phenyl) boronic acid (**3**). **NyDPAc** was further purified by train sublimation under reduced pressure ($<10^{-4}$ Torr). Details of their syntheses and purification are provided in the Supporting Information.

3.3. Photophysical properties

We investigated the photophysical properties using ultraviolet–visible (UV–vis), photoluminescence (PL), and transient PL spectroscopy. The photophysical properties of **NyDPAc** are summarized in Table 2. In the UV–vis spectra, charge transfer (CT) absorption occurred at 350 nm, which represents the charge transfer from

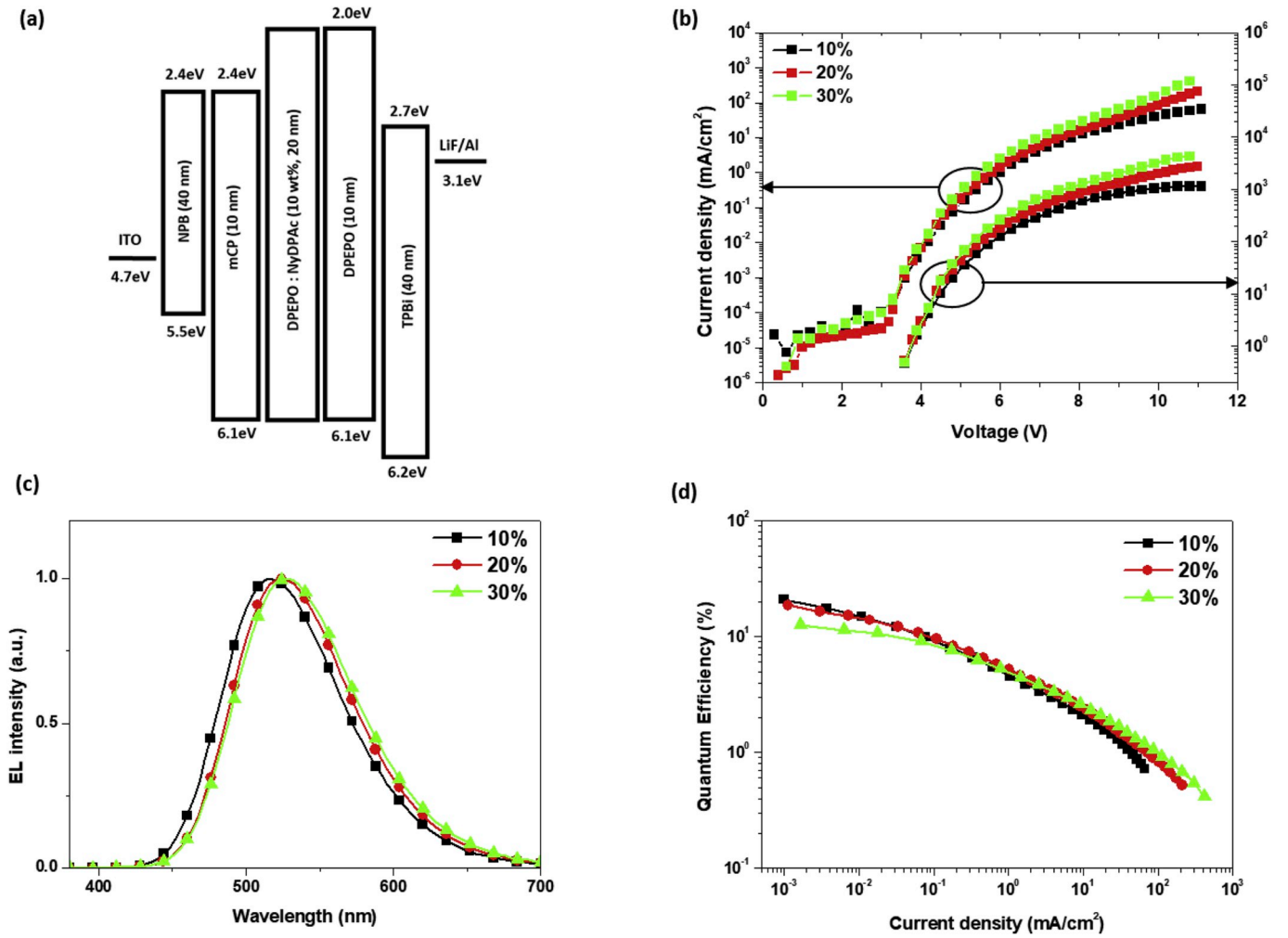

Fig. 3. (a) Energy level diagram for the OLED device, (b) current density-voltage-luminance (J-V-L) curves, (c) EL spectra at 5 V, (d) external quantum efficiency-current density (η_{EQE}-J) curve.

dimethylacridine to naphthyridine. As a result, solvatochromism appeared as the polarity of the solvent increased from toluene to tetrahydrofuran (THF) and methylene chloride (MC). The CT emissions were observed at 486 nm in toluene, 548 nm in THF, and 558 nm in MC (Fig. 2a). Thin-film PL measurements were conducted using bis[2-(diphenylphosphino)phenyl] ether oxide (DPEPO) as a host with a high T_1 energy (T_1 = 3.0 eV) [26]. The 10 wt% doped film exhibited CT emission at 510 nm and an absolute PLQY of 57%.

The time-gated PL spectra were acquired at a low temperature (77 K) to investigate the characteristics of triplet excited states (Fig. 2b). Both solution and film phosphorescence spectra were characterized by the mixing of ^{3}CT and ^{3}LE states [27], compared to the spectrum of the acceptor moiety (Fig. S1), whereas the fluorescence has a ^{1}CT character. ΔE_{ST} was estimated to be approximately 0.30 eV based on the onset of spectra. To confirm the TADF characteristics, a transient PL decay profile of **NyDPAc** in the doped films was obtained (Fig. 2c). Decay curves showed prompt and delayed components with lifetimes of 12 ns and 451 μs, respectively. **NyDPAc** clearly showed TADF emission despite large ΔE_{ST}. This was due to appropriate interactions between ^{1}CT, ^{3}LE, and ^{3}CT for RISC according to the El-Sayed rule [28]. In fact, several studies on successful TADF emitters have been conducted using large ΔE_{ST} [29–32]. The kinetic constants of **NyDPAc** were calculated according to the Adachi's method (Table S1) [33–35].

Table 3
Device data of **NyDPAc** in a DPEPO host matrix.

Doping concentration	Turn on voltage [V]	EQE_{max} [a] [%]	CE [b] [cd A^{-1}]	PE [c] [lm W^{-1}]	CIE Coordinates [d] (x, y)	λ_{max} [e] [nm]
10%	3.6	20.9	47.9	41.8	0.28, 0.53	516
20%	3.6	18.7	46.1	40.2	0.30, 0.55	524
30%	3.6	12.6	29.8	26.0	0.32, 0.55	528

[a] External quantum efficiency.
[b] Current efficiency.
[c] Power efficiency.
[d] CIE 1931 Coordinates.
[e] Maximum wavelength at 5V.

3.4. Electrochemical and thermal properties

The HOMO and LUMO levels of **NyDPAc** measured by cyclic voltammetry were 5.30 and 2.87 eV, respectively (Fig. S2). Therefore, DPEPO (HOMO = 6.1 eV, LUMO = 2.0 eV) can serve as a suitable host material for **NyDPAc**. Differential Scanning calorimetry (DSC) and thermal gravimetric analysis (TGA) showed extremely high thermal stability with a glass transition temperature (T_g) of 144 °C and a decomposition temperature (T_d) of 414 °C at 5% weight loss (Fig. S3).

3.5. Device properties

The OLED device structure was as follows (Fig. 3a): indium tin oxide (ITO, 150 nm)/*N*,*N*′-di(1-naphthyl)-*N*,*N*′-diphenyl-(1,1′-biphenyl)-4,4′-diamine (NPB, 40 nm)/1,3-bis(*N*-carbazolyl)benzene (mCP, 10 nm)/DPEPO:**NyDPAc** (20 nm, x wt%)/DPEPO (10 nm)/2,2′,2"-(1,3,5-benzinetriyl)-tris(1-phenyl-1-*H*-benzimidazole(TPBi, 40 nm)/LiF (1 nm)/Al (100 nm). The device data are summarized in Table 3. The device showed an emission peak of 516 nm, an EQE_{max} of 20.9%, a current efficiency (CE) of 47.9 cd A^{-1}, a power efficiency (PE) of 41.8 lm W^{-1}, and CIE coordinates of (0.28, 0.53) at 10% doped **NyDPAc**. As the concentration of dopant increased, we observed decreased EQEs and emission spectral shifts, which are presumably due to the interactions between emitter molecules [36]. The long TADF lifetime of **NyDPAc** (451 μs, Table 2) resulted in large device efficiency roll-off (Fig. 3d) [37,38]. Interestingly, the calculated EQE was 11.4% based on the PLQY of 57% and light out-coupling efficiency of 20%. However, the obtained EQE of 20.9% was much higher than the calculated value.

To obtain greater insight into the unexpected high EQE, the angle-dependent PL of p-polarized light was measured using a 30-nm-thick film of 10 wt% **NyDPAc** in DPEPO to investigate the emitting dipole orientation (EDO) (Fig. 2d). The EDO ratio was obtained by fitting the measured curves to the classical dipole optical simulation. **NyDPAc** showed 92% of the horizontal EDO ratio ($\Theta_{//}$), indicating that **NyDPAc** had a fairly good horizontal orientation in the layer of DPEPO. Based on the PLQY and $\Theta_{//}$ of **NyDPAc**, the theoretical maximum EQE was calculated through optical simulation, assuming that the thickness of the ITO was 150 nm and $\Phi_{RISC} = 1$. Calculations showed that the EQE could reach 20.6%, which is nearly identical to our experimental results. EDO and simulation verified that **NyDPAc** was well arranged in the horizontal orientation. Thus, the increased EQE clearly originated from the high horizontal orientation.

4. Conclusion

In conclusion, the TADF emitter **NyDPAc** containing 1,5-naphthyridine as an electron acceptor showed TADF emission and high horizontal dipole orientation. The distinct ^{1}CT and ^{3}LE emission of **NyDPAc** resulted in RISC for TADF, thus improving the EQE. The high horizontal EDO ratio of **NyDPAc** further increased the EQE by enhancing the light out-coupling efficiency. Device data (10 wt% doped) showed a high EQE of 20.9%, a CE of 47.9 Cd A^{-1}, and a PE of 41.8 lm W^{-1}. Our study suggests that using 1,5-naphthyridine as a core moiety is an effective means of developing efficient TADF emitters. Further modified design based on the 1,5-naphthyridine structure is currently underway in our laboratory.

Declaration of competing interest

The authors declare that they have no known competing financial interests or personal relationships that could have appeared to influence the work reported in this paper.

Acknowledgement

This work was supported by the NRF grant (No. 2018R1A2B2001293) funded by the MSIP.

Appendix A. Supplementary data

Supplementary data to this article can be found online at https://doi.org/10.1016/j.orgel.2019.105600.

References

[1] M.A. Baldo, D.F. O'Brien, Y. You, A. Shoustikov, S. Sibley, M.E. Thompson, et al., Highly efficient phosphorescent emission from organic electroluminescent devices, Nature 395 (6698) (1998) 151–154.
[2] C. Adachi, M.A. Baldo, M.E. Thompson, S.R. Forrest, Nearly 100% internal phosphorescence efficiency in an organic light-emitting device, J. Appl. Phys. 90 (10) (2001) 5048–5051.
[3] L.J. Rothberg, A.J. Lovinger, Status of and prospects for organic electroluminescence, J. Mater. Res. 11 (12) (1996) 3174–3187.
[4] R.H. Friend, R.W. Gymer, A.B. Holmes, J.H. Burroughes, R.N. Marks, C. Taliani, et al., Electroluminescence in conjugated polymers, Nature 397 (6715) (1999) 121–128.
[5] H. Uoyama, K. Goushi, K. Shizu, H. Nomura, C. Adachi, Highly efficient organic light-emitting diodes from delayed fluorescence, Nature 492 (2012) 234.
[6] Y.-Z. Shi, K. Wang, X. Li, G.-L. Dai, W. Liu, K. Ke, et al., Intermolecular charge-transfer transition emitter showing thermally activated delayed fluorescence for efficient non-doped OLEDs, Angew. Chem. Int. Ed. 57 (30) (2018) 9480–9484.
[7] H. Mieno, R. Kabe, M.D. Allendorf, C. Adachi, Thermally activated delayed fluorescence of a Zr-based metal–organic framework, Chem. Commun. 54 (6) (2018) 631–634.
[8] Y. Xiang, Z.-L. Zhu, D. Xie, S. Gong, K. Wu, G. Xie, et al., Revealing the new potential of an indandione unit for constructing efficient yellow thermally activated delayed fluorescence emitters with short emissive lifetimes, J. Mater. Chem. C 6 (26) (2018) 7111–7118.
[9] C. Li, C. Duan, C. Han, H. Xu, Secondary acceptor optimization for full-exciton radiation: toward sky-blue thermally activated delayed fluorescence diodes with external quantum efficiency of ≈30%, Adv. Mater. 30 (50) (2018) 1804228.
[10] S.-J. Woo, Y. Kim, Y.-H. Kim, S.-K. Kwon, J.-J. Kim, A spiro-silafluorene–phenazasiline donor-based efficient blue thermally activated delayed fluorescence emitter and its host-dependent device characteristics, J. Mater. Chem. C 7 (14) (2019) 4191–4198.
[11] W. Brütting, J. Frischeisen, T.D. Schmidt, B.J. Scholz, C. Mayr, Device efficiency of organic light-emitting diodes: progress by improved light outcoupling, Phys. Status Solidi A 210 (1) (2013) 44–65.
[12] A. Endo, K. Sato, K. Yoshimura, T. Kai, A. Kawada, H. Miyazaki, et al., Efficient up-conversion of triplet excitons into a singlet state and its application for organic light emitting diodes, Appl. Phys. Lett. 98 (8) (2011), 083302.
[13] A. Senes, S.C.J. Meskers, H. Greiner, K. Suzuki, H. Kaji, C. Adachi, et al., Increasing the horizontal orientation of transition dipole moments in solution processed small molecular emitters, J. Mater. Chem. C 5 (26) (2017) 6555–6562.
[14] D. Yokoyama, Molecular orientation in small-molecule organic light-emitting diodes, J. Mater. Chem. 21 (48) (2011) 19187–19202.
[15] Y.J. Cho, B.D. Chin, S.K. Jeon, J.Y. Lee, 20% external quantum efficiency in solution-processed blue thermally activated delayed fluorescent devices, Adv. Funct. Mater. 25 (43) (2015) 6786–6792.
[16] Y. Wada, K. Shizu, S. Kubo, K. Suzuki, H. Tanaka, C. Adachi, et al., Highly efficient electroluminescence from a solution-processable thermally activated delayed fluorescence emitter, Appl. Phys. Lett. 107 (18) (2015) 183303.
[17] M. Kim, S.K. Jeon, S.-H. Hwang, S.-S. Lee, E. Yu, J.Y. Lee, Correlation of molecular structure with photophysical properties and device performances of thermally activated delayed fluorescent emitters, J. Phys. Chem. C 120 (5) (2016) 2485–2493.
[18] S.Y. Byeon, J. Kim, D.R. Lee, S.H. Han, S.R. Forrest, J.Y. Lee, Nearly 100% horizontal dipole orientation and upconversion efficiency in blue thermally activated delayed fluorescent emitters, Advanced Optical Materials 6 (15) (2018) 1701340.
[19] W. Li, B. Li, X. Cai, L. Gan, Z. Xu, W. Li, et al., Tri-spiral donor for high efficiency and versatile blue thermally activated delayed fluorescence materials, Angew. Chem. Int. Ed. 58 (33) (2019) 11301–11305.
[20] X. Zeng, K.-C. Pan, W.-K. Lee, S. Gong, F. Ni, X. Xiao, et al., High-efficiency pure blue thermally activated delayed fluorescence emitters with a preferentially horizontal emitting dipole orientation via a spiro-linked double D–A molecular architecture, J. Mater. Chem. C 7 (35) (2019) 10851–10859.
[21] T. Komino, H. Tanaka, C. Adachi, Selectively controlled orientational order in linear-shaped thermally activated delayed fluorescent dopants, Chem. Mater. 26 (12) (2014) 3665–3671.
[22] D.H. Kim, K. Inada, L. Zhao, T. Komino, N. Matsumoto, J.C. Ribierre, et al., Organic light emitting diodes with horizontally oriented thermally activated delayed fluorescence emitters, J. Mater. Chem. C 5 (5) (2017) 1216–1223.
[23] G. Roma, M. Di Braccio, G. Grossi, F. Mattioli, M. Ghia, 1,8-Naphthyridines IV. 9-substituted N,N-dialkyl-5-(alkylamino or cycloalkylamino) [1,2,4]triazolo[4,3-a] [1, 8]naphthyridine-6-carboxamides, new compounds with anti-aggressive and potent anti-inflammatory activities, Eur. J. Med. Chem. 35 (11) (2000) 1021–1035.
[24] D.J. Hazuda, N.J. Anthony, R.P. Gomez, S.M. Jolly, J.S. Wai, L. Zhuang, et al., A naphthyridine carboxamide provides evidence for discordant resistance between mechanistically identical inhibitors of HIV-1 integrase, Proc. Natl. Acad. Sci. U. S. A. 101 (31) (2004) 11233–11238.
[25] K.M. Peese, C.W. Allard, T. Connolly, B.L. Johnson, C. Li, M. Patel, et al., 5,6,7,8-Tetrahydro-1,6-naphthyridine derivatives as potent HIV-1-Integrase-Allosteric-Site inhibitors, J. Med. Chem. 62 (3) (2019) 1348–1361.
[26] C. Han, Y. Zhao, H. Xu, J. Chen, Z. Deng, D. Ma, et al., A simple phosphine–oxide host with a multi-insulating structure: high triplet energy level for efficient blue electrophosphorescence, Chem. Eur J. 17 (21) (2011) 5800–5803.

[27] T. Hosokai, H. Matsuzaki, H. Nakanotani, K. Tokumaru, T. Tsutsui, A. Furube, et al., Evidence and mechanism of efficient thermally activated delayed fluorescence promoted by delocalized excited states, Science Advances 3 (5) (2017), e1603282.
[28] P.K. Samanta, D. Kim, V. Coropceanu, J.-L. Brédas, Up-Conversion intersystem crossing rates in organic emitters for thermally activated delayed fluorescence: impact of the nature of singlet vs triplet excited states, J. Am. Chem. Soc. 139 (11) (2017) 4042–4051.
[29] T. Takahashi, K. Shizu, T. Yasuda, K. Togashi, C. Adachi, Donor–acceptor-structured 1,4-diazatriphenylene derivatives exhibiting thermally activated delayed fluorescence: design and synthesis, photophysical properties and OLED characteristics, Sci. Technol. Adv. Mater. 15 (3) (2014), 034202.
[30] X. Cai, X. Li, G. Xie, Z. He, K. Gao, K. Liu, et al., "Rate-limited effect" of reverse intersystem crossing process: the key for tuning thermally activated delayed fluorescence lifetime and efficiency roll-off of organic light emitting diodes, Chem. Sci. 7 (7) (2016) 4264–4275.
[31] P. Data, P. Pander, M. Okazaki, Y. Takeda, S. Minakata, A.P. Monkman, Dibenzo[a,j]phenazine-Cored donor–acceptor–donor compounds as green-to-red/NIR thermally activated delayed fluorescence organic light emitters, Angew. Chem. Int. Ed. 55 (19) (2016) 5739–5744.
[32] S.G. Yoo, W. Song, J.Y. Lee, Molecular engineering of donor moiety of donor–acceptor structure for management of photophysical properties and device performances, Dyes Pigments 128 (2016) 201–208.
[33] Q. Zhang, H. Kuwabara, W.J. Potscavage, S. Huang, Y. Hatae, T. Shibata, et al., Anthraquinone-based intramolecular charge-transfer compounds: computational molecular design, thermally activated delayed fluorescence, and highly efficient red electroluminescence, J. Am. Chem. Soc. 136 (52) (2014) 18070–18081.
[34] Q. Zhang, B. Li, S. Huang, H. Nomura, H. Tanaka, C. Adachi, Efficient blue organic light-emitting diodes employing thermally activated delayed fluorescence, Nat. Photonics 8 (2014) 326.
[35] S. Oda, B. Kawakami, R. Kawasumi, R. Okita, T. Hatakeyama, Multiple resonance effect-induced sky-blue thermally activated delayed fluorescence with a narrow emission band, Org. Lett. 21 (23) (2019) 9311–9314.
[36] H.S. Kim, S.-R. Park, M.C. Suh, Concentration quenching behavior of thermally activated delayed fluorescence in a solid film, J. Phys. Chem. C 121 (26) (2017) 13986–13997.
[37] K. Masui, H. Nakanotani, C. Adachi, Analysis of exciton annihilation in high-efficiency sky-blue organic light-emitting diodes with thermally activated delayed fluorescence, Org. Electron. 14 (11) (2013) 2721–2726.
[38] Z. Yang, Z. Mao, Z. Xie, Y. Zhang, S. Liu, J. Zhao, et al., Recent advances in organic thermally activated delayed fluorescence materials, Chem. Soc. Rev. 46 (3) (2017) 915–1016.